

Avalanche gain and its effect on energy resolution in GEM-based detectors

T. N. Thorpe^{1,*}, S. E. Vahsen

Department of Physics and Astronomy, University of Hawaii, Honolulu, HI 96822, USA

Abstract

Gas Electron Multipliers (GEMs) are gas avalanche devices that have been enabled by modern photo-lithography. Compared to traditional multi wire proportional chambers, GEMs offer smaller feature size and higher rate capabilities. When designing GEM-based detectors, often a large parameter space of gas mixtures, GEM specifications, and operational parameters needs to be considered. In this context, a description which parameterizes the gain and the energy resolution to include these quantities is valuable for efficient detector design optimization and interpretation of results. We present avalanche gain and associated pulse-height resolution measurements recorded with a ⁴He:CO₂ (70:30) gas mixture and pure SF₆, a Negative Ion (NI) gas. SF₆ is of particular interest to the directional dark matter community, as its low thermal diffusion helps to retain recoil ionization track information over large drift lengths. With some review, and the aid of a general form of the first Townsend coefficient, multiple GEM-based detector data sets are used to study gas gain across a large reduced field, E/p , range. The high-gain behavior, where detector or readout electronics noise becomes negligible, of the electron drift gas is well described purely in terms of experimental parameters relevant for GEM-based detectors. Operation at high gain is an important consideration for experiments involved in low-energy, rare-event searches. The pulse-height resolution measurements are also used to discuss the variance of the avalanche distribution and to describe the lower limits of energy resolution one should expect to measure. In the end, a more comprehensive understanding of avalanche gain, its effect on energy resolution, and the contributing experimental parameters in GEM-based detectors is developed for further use.

Keywords: GEM, gas gain, energy resolution, Townsend, avalanche variance, Negative Ion, SF₆

1. Introduction

Gas Electron Multipliers (GEMs) [1] are widely used in the detection of elementary particles. Their robustness and improved performance over traditional multi-wire proportional chambers (MWPCs) have led to many modern experiments utilizing gaseous time projection chambers (TPCs) [2] with charge readouts based on GEMs [3–5]. GEMs are a form of Micro Pattern Gaseous Detector (MPGD) owing to their small feature size. When coupled with highly segmented detection elements, GEM-based detectors can produce high definition 3d images of individual ionization events [6] where the avalanche gain and its effect on energy resolution play an important role. The measurements presented here are the byproduct of gas component and gain optimization studies for directional neutron detection [7, 8], the Directional Dark Matter Detector D³ [6, 9–12], and the wider CYGNUS [13] and directional recoil detection [14] efforts at the University of Hawaii. The parameterization and analysis methods presented here are broadly applicable to GEM-based detectors, or any gas avalanching devices utilizing a uniform electric field. The present work spans multiple years and experimental setups with improvements being imple-

mented over time, and a concerted effort has been taken to account for numerous systematic issues. Full details can be found in Ref. [15].

GEMs exploit the principle of gas avalanching, or Townsend avalanching, where free electrons are accelerated by a strong electric field. These accelerating electrons undergo collisions with other, atomically bound electrons within the chosen gas mixture, freeing them. These newly freed electrons are then accelerated and continue the process, thus creating an ‘avalanche’ of charge, which can be macroscopic and measured. The ratio of this macroscopic charge pulse to the amount of charge in the initial ionization cloud is commonly referred to as the *gas gain*. Each primary electron will generate its own avalanche, each with its own unique properties. As there are generally many electrons in the initial ionization cloud, the magnitude of the resulting charge pulse from the sum of all of those avalanches will have a variance. This variance in the charge avalanche distribution, or simply the *avalanche variance*, and it is one of the major contributions to the pulse-height resolution. It also places a fundamental limit on the energy resolution achievable in GEM-based detectors. This, along with the gas gain, are primary considerations in detector design and are the central topics of the present work.

The gas gain process is stochastic in nature and complicated by many microscopic effects including gas impurities, non-ionizing collisions, saturation effects, and Penning effects in

*Corresponding author. Tel.: +41227679281

Email address: tnthorpe@g.ucla.edu (T. N. Thorpe)

¹Now at Department of Physics and Astronomy, University of California - Los Angeles, 475 Portola Plaza, Los Angeles, CA 90095

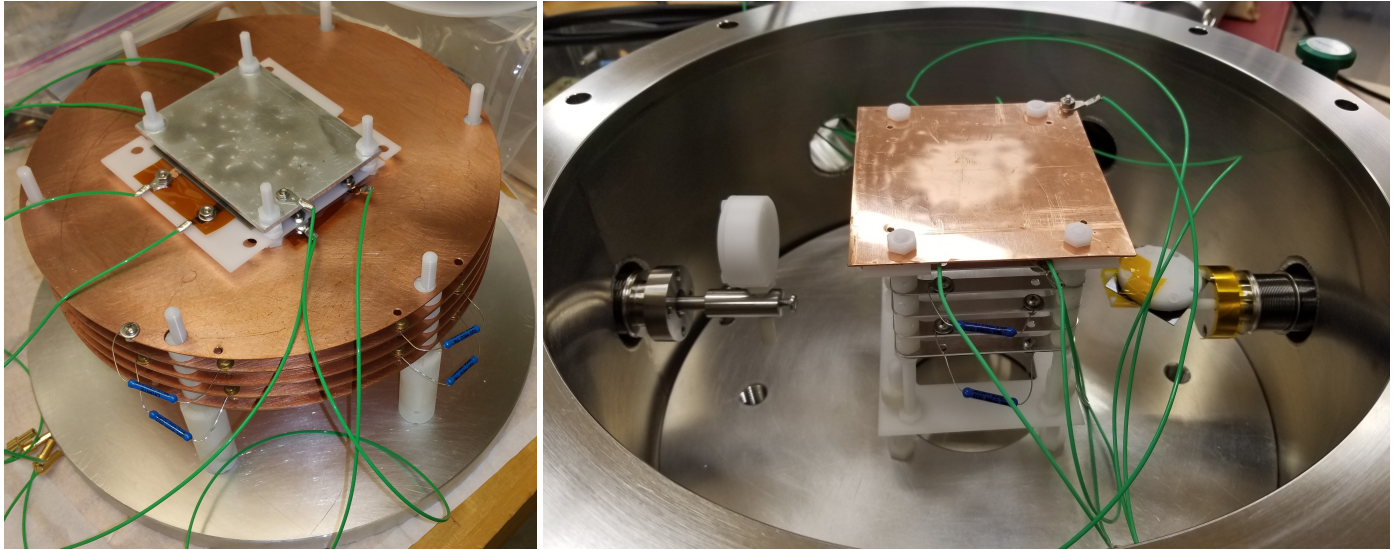


Figure 1: Experimental apparatus used for measurements. Left: Structure for the 3-tGEM and the 1-THGEM setups, which used larger components and had higher material outgassing as a result. Right: The 2-tGEM and 2-THGEM setups, which used less material and provided a very stable environment. The white disk facing up on the far right is the collimated holder for the ^{55}Fe source which can be moved laterally to perform both source and background measurements. The aluminum (left) and copper (right) charge collection plates can be seen mounted on the top of both structures, and charge is drifted upwards in all setups.

Setup name	GEM assembly	Gas Used (sections discussed)	Drift	Transfer 1	Transfer 2	Collection
2-tGEM	2 thin GEMs	$^4\text{He}:\text{CO}_2$ (4.3, 5.3)	4.53	0.13	n/a	0.16
3-tGEM	3 thin GEMs	$^4\text{He}:\text{CO}_2$ (4.3, 5.3)	4.92	0.28	0.28	0.23
1-THGEM	1 THGEM	$^4\text{He}:\text{CO}_2$ (4.3, 5.3) and SF_6 (4.2, 5.2)	5.14	n/a	n/a	0.18
2-THGEM	2 THGEMs	$^4\text{He}:\text{CO}_2$ (4.3, 5.3)	4.72	0.09	n/a	0.13

Table 1: GEM setups and gases used. The proportion of the $^4\text{He}:\text{CO}_2$ mixture is 70:30, while SF_6 is pure. The dimensions (cm) of the drift, transfer, and collection regions are also listed. The GEM specifications are provided in Table 2.

mixtures. There are computer simulation programs [16] which exploit the Monte Carlo technique and take these effects into account to varying degrees for gain calculations. However, producing and validating such simulations for many experimental setups is time consuming, and this is not our goal here. We instead take a simpler, data-driven approach to parametrizing and interpreting our results.

The first Townsend coefficient, α , quantifies a charge avalanche's growth and has units of number per length. The gas pressure, p , and electric field strength, E , within a GEM can be combined into a single quantity, E/p , referred to as the reduced electric field or simply the *reduced field*. The reduced field along with the number of GEMs, n_g , used for charge amplification can be used to describe the avalanche gain via α . By considering the average electric field strength in a generic GEM-based gain stage, along with a general form for the first Townsend coefficient, we show that gas gain data from multiple detector setups is well described over a large parameter space. This is done using gas mixtures, $^4\text{He}:\text{CO}_2$ (70:30) and $\text{Ar}:\text{CO}_2$ (70:30), and pure SF_6 .

Throughout this work, gain values are obtained from pulse-height distributions. Substantial use is also made of the associated pulse-height (PH) resolutions, i.e. the sigma divided by the mean of the distribution. We consider the various contributions to the PH resolution, and ultimately the energy resolu-

tion, and seek methods to minimize them. We do this by defining the *asymptotic gain* as the high-gain value where any electronic readout induced noise is suppressed. Then, using multiple asymptotic gain values from different GEM-based detector data sets we show that PH resolution retains a gain and reduced field dependence. This is attributed to dependence of the avalanche variance on the gain and reduced field, and we confirm that this effect is minimized as the average reduced field in the GEM(s) is increased. A method describing this relationship is provided and discussed with data from a $^4\text{He}:\text{CO}_2$ (70:30) gas mixture.

Within the Directional Dark Matter (DDM) community, gaseous TPCs remain the most mature technology and the gas gain and associated energy resolution are of primary importance when detector design is considered. Currently, the most powerful discrimination technique utilizes high signal-to-noise (SNR) detector schemes coupled with highly segmented readouts to measure the difference between the ionization track topologies from nuclear (signal) and electron (background) recoils. At low ionization energies, $\mathcal{O}(1\text{-}10\text{ keV})$, such discrimination becomes difficult and the detection of every primary electron becomes crucial. For a GEM-based TPC this means running at or above the asymptotic gain, so the parameterization and analysis methods presented here are particularly relevant. A good energy resolution is crucial for directional DM searches

of these dividers. The exception is the 2-tGEM setup, which used fewer field cage rings (2 cm spacing) each with its own HV channel.

Generally, the GEMs are powered via an independent HV supply (HV - GEM) and an external resistive divider (HV Box) which is outlined in red in Fig. 2. This is done to free up HV channels and to provide 100 M Ω protection resistors for the GEMs. Resistor values, and the number of HV channels used, were changed as needed given the requirements of a particular GEM setup. However, Fig. 2 is a good representation of the electrical scheme used in all cases, and relevant information about the electric fields will be provided as needed.

One important characteristic common to all of the HV dividers is that the transfer and collection fields are proportional to the total voltage across all of the GEMs, V_G , so the transfer and collection fields change as some proportion of V_G , with the constant of proportionality depending in the specific setup. However, all of the drift fields are powered by a separate HV supply (HV - Drift) and are independently controlled. Multiple different power supplies are used for the various setups, including a Keithley model 248 (5 kV), a Stanford Research Systems model PS370 (20 kV), and a CAEN NDT1470 (8 kV). These models were chosen for their low jitter. Gas gain has an exponential dependence on the GEM voltage, so an accurate and stable voltage is always desired.

2.3. Data acquisition

For all measurements a conductive, charge collection plate is used on a single readout channel. This is labeled as ‘Readout plate’ in Fig. 2. By doing this we are not introducing any additional geometric or threshold effects that more sophisticated, segmented readouts will which contribute to the energy resolution at all gain values. These additional effects [23] can be difficult to account for because they generally result in charge that is not collected, the amount of which is hard to know. This is important because (disregarding the possibility of counting single electrons [24]) once detector and other noise effects are minimized, the PH resolution can be thought of as a minimum value of the energy resolution that a detector can achieve.

Conversely, our charge collection plate is a single piece of aluminum or copper which measures approximately (5 cm)² and its purpose is to ensure that all of the avalanched charge from the GEM is collected. However, a large gain-independent noise term results, acting as a ‘noise floor’ below which measurements are not possible. This noise hinders measurements with low signal-to-noise ratios (SNR) which, in the present case, are low gain signals. Note that sources which create a large initial ionization signal can still provide a high SNR at low gain.

The box labeled ‘DAQ’ in Fig. 2 contains everything downstream of the charge collection plate: an Endicott eV-5093 or a Cremat CR-110 charge sensitive preamplifier with respective gains of 3.6 V/pC and 1.4 V/pC. The preamp is housed inside an Endicott eV-550 module which greatly reduces the RF-noise and provides AC-coupling to the detector. Following the preamp, the signal is shaped by a Canberra AFT 2025 spectroscopy amplifier, and finally an Ortec EASY-MCA operates

as a Pulse Height Analyzer (PHA) digitizing the data for storage. Individual waveforms were continuously monitored with an oscilloscope as well, but only the pulse-height data is presented here.

2.4. Detector calibration

The detectors are calibrated by injecting voltage pulses into an approximately 1 pF test capacitor and measuring the output either at the shaping amplifier, or the corresponding bin number of the PHA. The ratio of either the magnitude of the output voltage pulse from the shaping amplifier or the PHA bin number to the magnitude of the injected voltage pulse is recorded as the system response. The setups pictured on the left and right of Fig. 1 have respective system responses of 0.91 V/pC and 2.86 PHA bins/fC. The PHA has an operating range of 0 - 10 V, which is divided into 8196 bins, and its linearity and repeatability were checked and monitored. Every resistive divider used to power the GEMs and field cages was carefully calibrated, and more details about the measurements of this and further systematic effects are provided in Section 4.4.

The different experimental setups have different system responses, whose values depend on the components in the chain of analog readout electronics. These values are directly proportional to, and used to determine, the gain from the pulse-height spectra. Uncertainty in these response measurements can originate from uncertainty in the measurement of the small injection capacitor, and this is well illustrated in data recorded with the 3-tGEM setup. The value used for these measurements is 0.91 V/pC and it has an uncertainty of approximately 14% due to the difficulty of measuring the small injection capacitance. This uncertainty is included throughout the results and analysis, notice the larger error bars on the data points from the 3-tGEM setup in Fig. 5.

Using the calibrated pulse-height scale, we can also estimate the magnitude of the aforementioned noise floor. We find that the level below which measurements are not possible is in the range of $O(10^4 - 10^5)$ electrons. If we assume that this is Johnson–Nyquist noise then this gives a capacitance of $O(100)$ nF for the noisiest setups. This is not unreasonable considering the size of the charge collection plate.

2.5. Measurement technique and procedure

The measurement process generally consists of pumping the vessel down to approximately 10^{-5} torr for at least a few hours, or a series of pump-and-purge cycles before filling. As the chamber reaches the desired pressure, the power supplies are turned on and the stability of the gas gain is monitored. Once suitable stability at a single GEM voltage is achieved, the GEM voltages can be varied and various measurements can be performed. Gain stability data sets are generally recorded for long periods surrounding other measurements, and this topic is discussed in detail in Section 4.4.2. We note that most of the measurements were performed without gas flowing through the vessel. However in a few instances, specifically with SF₆, gas flow was required. Gas flow and purity issues are explicitly discussed where appropriate.

GEM type	Thickness	Active area	Hole diameter	Pitch	Rim
Thin GEM (tGEM)	0.005	5 × 5	0.007	0.0014	n/a
Thick GEM (THGEM)	0.04	5 × 5	0.03	0.05	0.005

Table 2: Specifications of the GEMs used in this work. Dimensions in cm.

Unless otherwise specified, pulse-height spectra are integrated over five minutes to account for any acute time variation of the gain, and to achieve a large statistical sample. The integrals of the five minute spectra are checked for similar values to ensure that the full distribution is being measured, and each spectrum is used to extract a single gain value. The ^{55}Fe source (5.9 keV) is always placed near the cathode pointing along the drift axis into the drift region centered on the GEM(s). All of the He:CO₂ and SF₆ spectra, with the exception the 3-tGEM data set, have been background subtracted by completing a time normalized non-source run. This feature was added at some point later in time, and not available for the earliest measurements.

3. Definition of quantities and formalism

In this section we define the gain, PH resolution, and other relevant quantities. We also develop formalism which is used to describe the data in the later sections.

3.1. Gain

The gas gain as described here is the result of the Townsend avalanching process where ionized electrons, accelerated via a reduced field greater than approximately 30 V/cm/torr, undergo collisions with other atomically bound electrons within the gas mixture resulting in their liberation, subsequent acceleration, and a continuation of the process.

3.1.1. Townsend's equation with GEMs

The first Townsend coefficient, α , is a parameter that quantifies the progression of a charge avalanche. In general, α is a function of the reduced field, E/p , and it has units of number per length. Townsend's equation uses α to describe the exponential growth of a charge avalanche over a path length r , and can be written as

$$\frac{dn}{n} = \alpha dr, \quad (1)$$

where n is the total number of electrons produced in the avalanche. The gas gain can be defined as the ratio of the total number of electrons produced in the avalanche to the number of electrons in the primary ionization cloud, n_0 ,

$$G := \frac{n}{n_0}. \quad (2)$$

We note that if all avalanches are presumed to be identical then this is equivalent to defining the gain as the number of electrons produced by a single electron avalanche.

In general the electric field is a function of r , and α needs to be integrated over the entire path length of the avalanche to include any field dependent effects. However, here we only consider the constant avalanching fields produced by GEMs. We consider a system with a number of GEMs n_g all with equal thickness, t . This system will produce a gain G for a voltage V_G applied evenly across all the GEMs, i.e the single GEM voltage is $V_{GEM} = V_G/n_g$. Under these assumptions, we may integrate Townsend's equation in the case of an arbitrary GEM gain stage as

$$\ln(G) = \alpha n_g t. \quad (3)$$

From this we can see that the gain is a purely exponential function of α . If, in addition, α is strictly proportional to the electric field strength in the GEM, E , then the gain will be a strictly exponential function of V_G . This is a common assumption in literature when analyzing GEM-based detector results. However, deviations from the proportional dependence of α on E will result in deviations of the exponential dependence of the gain on V_G . Thus the next step is to express α in terms of the experimental parameters, E/p and n_g .

3.1.2. The reduced first Townsend coefficient

By defining α as the product of the number of mean free paths along the field direction that an ionized electron can take and the probability that a mean free path is larger than the mean free path for ionization, Ref. [25] provides a generalization of the 'reduced' first Townsend coefficient, α/N . It is written as a function of the reduced field, E/N ,

$$\frac{\alpha}{N} = K \left(\frac{E}{N} \right)^m \exp \left(-L \left(\frac{N}{E} \right)^{1-m} \right), \quad (4)$$

where E is the electric field strength, N is the gas density, and K , L , and m are experimentally fitted parameters related to the gas mixture. Assuming an ideal gas, Eq. 4 can be rewritten in terms of the gas pressure, p , as

$$\frac{\alpha}{p} = A \left(\frac{E}{p} \right)^m \exp \left(-B \left(\frac{p}{E} \right)^{1-m} \right), \quad (5)$$

where A and B have replaced K and L , respectively, and take into account the gas temperature. One underlying assumption to note is that the cross section of interaction between the accelerating electron and an atomically bound electron is proportional to $(E/p)^m$, with $0 \leq m \leq 1$. Many of the historical, and empirical, relationships describing gas gain data are simple manifestations of Eq. 5. For example, Diethorn's assumption

was that $\alpha \propto E$, or that $m = 1$ [26], and Williams and Sara used a more general form where $m = 0$ [27].

We can combine Eq. 3 with Eq. 5 to obtain

$$\frac{\ln(G)}{n_g p t} = A \left(\frac{V_G}{n_g p t} \right)^m \exp \left(-B \left(\frac{n_g p t}{V_G} \right)^{1-m} \right). \quad (6)$$

Eq. 6 now expresses the gas gain in a GEM-based detector entirely in terms of relevant experimental parameters. We will now do a bit of refining and further exploitation of this result.

3.1.3. Reduced quantities

To facilitate further discussion of Eq. 6, the following quantities are defined:

$$\Sigma := \frac{V_G}{n_g p t} \quad \text{and} \quad \Gamma := \frac{\alpha}{p} = \frac{\ln(G)}{n_g p t}, \quad (7)$$

where Σ is the reduced avalanching field strength in the gain stage averaged over the number of GEMs. When there is no ambiguity, this will be simply referred to as the reduced field. Γ is the reduced first Townsend coefficient (RFTC). Equation 6 can then be expressed as

$$\Gamma = A \Sigma^m e^{-B \Sigma^{m-1}}. \quad (8)$$

We will now discuss the limiting case of setting $m = 1$ in Eq. 8.

3.1.4. Gain versus total GEM voltage

Empirically, the dependence of the gain on V_G for a given detector setup is well described by

$$G = 10^{(V_G - V_1)/V_2}. \quad (9)$$

V_1 and V_2 are returned fit parameters and they provide useful intuition about the behavior of a given detector setup at a given gas pressure. V_1 is the voltage at which the gain is unity and V_2 is the voltage required to increase the gain by an order of magnitude. Equation 9 will be employed throughout Section 4. Such equations are often used when studying the results from GEM-based detectors, are sometimes referred to a detector's 'gain curve', and it's important to understand their origins.

Setting $m = 1$ in Eq. 8 is equivalent to saying that $\alpha/p \sim E/p$ which is equivalent to saying that $\ln(G)/n_g p t \sim V_G/n_g p t$, in the case of GEMs. Thus Eq. 9 is the equivalent of Eq. 8 when setting $m = 1$ and adding a voltage offset. We can further write

$$\Gamma = (\Sigma - \Sigma_1)/V_3, \quad (10)$$

where Σ_1 and V_3 are fit parameters that play the same role as V_1 and V_2 in Eq. 9. Σ_1 is the reduced field required to achieve zero RFTC and V_3 is the voltage required to increase the RFTC by unity (we use 1/cm/torr for the RFTC units). We also note that Eq. 10 allows for a negative RFTC at zero reduced field, which is not physical. A similar relationship was first used by

Zastawny to describe gas gain data with a uniform field in CO₂ [28].

Without this offset, Eq. 10 would imply a gain of unity at zero reduced field, passing through the origin of Γ versus Σ . In addition, it would describe a linear relationship between these two quantities fixed at the origin. This would imply relatively large gain values are low reduced fields, which is not observed in data. Adding the offset allows for a good description of the data, but implies a gain of unity at some non-zero field. This acts as a threshold, and we will refer to Eq. 10 as the *threshold model*.

The major drawback of the threshold model is that it provides minimal information about the gas mixture, and returns operational parameters. However, we will see that setting $m = 0$ in Eq. 8 provides an equally valid description without the need for the voltage offset, while also giving access to more information about the gas itself in the form of the parameters A and B .

A good rule of thumb summarizing this discussion can be stated as follows: The RFTC is proportional to the reduced field in the GEM. When a single gas pressure, GEM thickness, and specific number of GEMs are considered this implies that the $\ln(G)$ is proportional to V_G . This statement is only strictly true when $m = 1$ in Eq. 8 but, as mentioned, $m = 1$ is not required for an adequate data description.

3.1.5. The avalanche distribution and reduced quantities

While Eq. 8 forgoes the many secondary effects taking place within the gas gain process, it still provides useful insight. We will now transition into a discussion about the PH resolution in a similar manner. We only consider the effect of ionization and combine the gain and avalanching field strength into a single quantity. Consider the minimum distance an ionized electron must travel in order to initiate an avalanche. This distance will be inversely proportional to the avalanching field strength within a given GEM, $V_G/n_g t$, and will tend make the avalanche distributions more peaked [29]. We can then multiply this minimum distance by α , which is a measure the number of electrons per unit length in the avalanche, to obtain a new quantity

$$\chi \propto \alpha \left(\frac{n_g t}{V_G} \right) = \frac{\ln(G)}{n_g t} \left(\frac{n_g t}{V_G} \right) = \frac{\Gamma}{\Sigma}. \quad (11)$$

Using Eq. 3 for α , we see that χ is proportional to the RFTC divided by the reduced field. Then, using Eq. 8 we can determine its dependence on the reduced field,

$$\chi \propto A \Sigma^{m-1} e^{-B \Sigma^{m-1}}. \quad (12)$$

This quantity is introduced because it has been shown to be related to the variance of the avalanche distribution [30]. We will next that the variance of the avalanche distribution is one of the major contributors to the PH resolution, and ultimately the energy resolution.

3.2. Pulse-height (PH) and energy resolution

There are multiple effects that contribute to events with identical ionization energy having a statistically fluctuating measured charge, thereby limiting the energy resolution of a GEM-based detector. We briefly discuss the main contributions relevant in our study, and how these manifest in the measured pulse-height spectra.

When the gain is measured with a charge collection plate and read out with a single channel, as done here, the measured PH resolution can essentially be reduced to three terms. The first is the Fano factor, which quantifies the variance of the initial ionization distribution. Without a single electron source, the Fano factor will be an inherent part of the measured PH resolution. The second term is the variance of the charge avalanche distribution, which is dependent on the reduced field and the gain but does have a minimum value. The third is a ‘detector’ noise term which is due to the collection plate and the analog, amplification electronics used, and appears to be independent of the gain in all setups. We refer to the square root of the quadrature sum of these three terms as the *PH resolution*, R .

There are additional effects that can broaden the PH resolution, including variance in gain between the GEM holes and variation in time. The latter is explicitly addressed in Section 4.4.2 and in Ref. [7], where a double thin GEM setup is combined with a highly segmented pixel chip readout that shows week-long, percent-level gain stability using α -particle measurements. As for the former, we have used highly stable HV supplies and a collimated ^{55}Fe source here, but the degree of the transverse diffusion in the charge cloud in the drift gap of similar detectors is addressed in Refs. [6], [12], and [23]. This is not of major concern for the current discussion.

We start this section by working to suppress the gain-independent noise. This is done by quantitatively defining the asymptotic gain and asymptotic resolution. Once the detector noise term is suppressed, the PH resolution can more properly be referred to as an energy resolution which consists of two terms. Next, we seek a method to minimize the variance of the avalanche distribution, which is the only remaining term dependent on the reduced field and gain. This is done by defining the asymptotic RFTC, and the result can be regarded as a minimum value of resolution achievable in a GEM-based detector, for a given gas mixture, at a given energy.

3.2.1. PH resolution versus gain, and asymptotic quantities

Empirically, the observed PH resolution, R , has a dependence on the gain itself. This is well described by

$$R = \sqrt{\left(\frac{a}{G}\right)^2 + b^2}, \quad (13)$$

where a and b are returned fit parameters, and G is the measured gain. The parameter a can be interpreted as a constant value, gain-independent detector noise term, while b is the asymptotic, fractional PH resolution achieved with high-gain operation. For the fractional resolution to approach b , the gain must be much

larger than the detector noise. To this end, we define the *asymptotic gain*:

$$G_\infty := 100 \times a, \quad (14)$$

as the gain at which the *asymptotic resolution*, b , can be ensured. Eq. 13 will be employed throughout Section 4.

3.2.2. Asymptotic, reduced quantities

Generally, with a given setup, multiple measurements are performed at different gains to establish detector performance trends. However, to compare multiple setups with each other, it is useful to identify a single set of points that describe a single detector setup well. With this in mind, we consider a particular detector operating at its asymptotic gain and define the asymptotic, reduced, GEM-averaged quantities

$$\Sigma_\infty := \frac{V_{G_\infty}}{n_g p t} \quad \text{and} \quad \Gamma_\infty := \frac{\ln(G_\infty)}{n_g p t}. \quad (15)$$

Σ_∞ is the asymptotic, reduced, avalanching field strength in the gain stage averaged over the number of GEMs. Γ_∞ is the RFTC at the detector’s asymptotic gain value. G_∞ is defined as above, where a is extracted from Eq. 13 after fitting to a particular setup’s resolution versus gain data. $V_{G_\infty} = \log(G_\infty)V_2 + V_1$ comes from Eq. 9, where V_1 and V_2 are extracted after fitting to the setup’s gain versus total GEM voltage data.

Σ_∞ and Γ_∞ will be referred to as the *asymptotic reduced field* and the *asymptotic RFTC*, respectively. These quantities help reduce the effect of the systematic differences between the detector setups. They are a reasonable choice as high gas gain operation, at or above the asymptotic values, is of interest for many communities including in low-energy, rare-event searches. These quantities are exploited in Section 5.3, where we consider data from multiple detector setups using the same gas over a large range of reduced field.

As mentioned previously, the variance of the avalanche distribution is not constant, and its dependence on the gain and the reduced field is complicated. However, by observing how the asymptotic resolution behaves as a function of the quantities defined in Eq. 15, we propose a new methodology for minimizing the PH resolution and, consequently, the energy resolution.

3.2.3. The minimum PH resolution

With the detector noise term suppressed at high gain, we are left to conclude that any further decrease in the resolution is a result of the avalanche variance decreasing at higher reduced field values. In Section 5.3, we will show using the He:CO₂ data that the asymptotic RFTC is essentially linear with the asymptotic reduced field, analogous to the relationship between the gain and the total GEM voltage, across a large parameter space. In Section 5.3.3, after correcting for the stability, we will also show that the asymptotic resolution has a relationship with the asymptotic RFTC that is analogous to the relationship between the PH resolution and the gain, i.e. Eq. 13. In anticipation we write

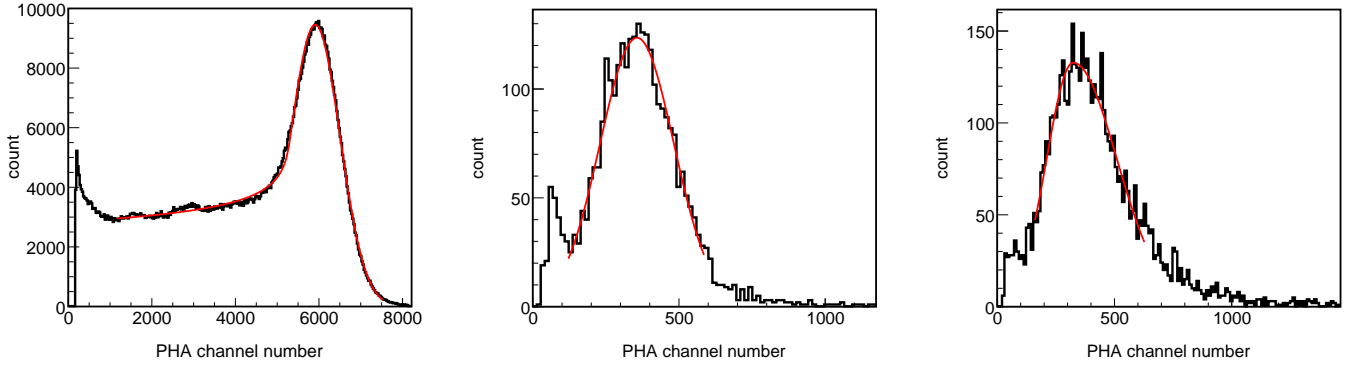


Figure 3: Examples of the pulse-height spectra obtained with an ^{55}Fe (5.9 keV) source from which the gain and PH resolution measurements are extracted. The solid lines (red online) are fits to the distributions. Left: A typical spectrum measured at high gain, $\approx 6 \times 10^4$, in $^4\text{He}:\text{CO}_2$ (70:30) with the 3-tGEM setup at atmospheric pressure. Center and right: SF_6 pulse-height spectra at a gain of approximately 2500 measured with the 1-THGEM setup at 20 torr (center) and 40 torr (right).

$$b \equiv R_\infty = \sqrt{\left(\frac{\mathcal{A}}{\Gamma_\infty}\right)^2 + \mathcal{B}^2}, \quad (16)$$

where \mathcal{A} is a term that is partially attributed to the avalanche variance being suppressed at higher asymptotic RFTC.

It should be noted that the analogy here with Eq. 13 is not perfect. The detector noise term in Eq. 13 was assumed to be independent of the gain, whereas the avalanche variance, and thereby \mathcal{A} , remains a function of the gain and the reduced field. However, this method still provides useful insight. In particular, \mathcal{B} can be interpreted as a measurement of the lower limit of the fractional energy resolution achievable in GEM-based detectors using a given gas mixture with a given initial ionization energy.

3.2.4. Variance of the avalanche distribution and the Fano factor

With the detector, gain, and reduced field-dependent effects minimized, we can be more explicit about the Fano factor and avalanche variance. We can also consider the dependence of the energy resolution on the initial ionization energy.

If each avalanche is assumed to be statistically independent, which is true for most of the proportional region, we can express the charge multiplication within the avalanche in terms of a single-electron avalanche factor, A . This allows us to write the fractional resolution as [30] [31]

$$R_\infty^2 = \left(\frac{\sigma_{n_0}}{n_0}\right)^2 + \frac{1}{n_0} \left(\frac{\sigma_A}{A}\right)^2, \quad (17)$$

where \bar{A} and n_0 are the average multiplication of a single electron and number of electrons in the primary ionization cloud, respectively.

The Fano factor, $F = \sigma_{n_0}^2/n_0$, is usually introduced to account for the fluctuations in the primary ionization. In addition, we denote the fractional avalanche variance as f , i.e. $f = (\sigma_A/\bar{A})^2$. Equation 17 can now be written as

$$R_\infty^2 = W \frac{(F + f)}{E_i}, \quad (18)$$

where E_i is the primary ionization energy. $W = E_i/n_0$ is known as the W-value, or W-factor, and it is the average amount of energy required to create an electron-ion pair and is energy dependent, but constant above a few keV [32]. For gases, typical values are approximately 30 eV.

F and f are the fundamental experimental parameters that govern the achievable lower limit of energy resolution at a given energy in ionization avalanching detectors. As described here, f represents the variance in the size of avalanches initiated by single electrons. The Fano factor describes how much of the incident particle's energy went into ionization and it approaches unity as this energy decreases toward the ionization potential of the gas, but is constant above a few keV with a slight dependence on the type of incident particle [32]. Equations 17 and 18 will be true regardless of the specific gain or reduced field values. However, lower gain values will generally produce avalanches with larger f values.

3.3. Remark about distributing the voltage across the GEMs

With the relationship between the gain, reduced field, and the PH resolution established, we mention a subtlety. Eq. 3 has the implicit assumption that the total voltage applied across all GEMs, V_G , is divided evenly between the number of GEMs, n_g . As shown in Table 4, V_G in our experiments is always within a few percent of being divided evenly amongst the number of GEMs within a given setup, but this is not always the case.

When considering only the gain though, this is not a major concern. As long as each GEM is biased enough to produce some gain, then each GEM will produce roughly the same proportion of $\ln(G)$ as the proportion of V_G that it is biased with. This is simply due to that fact that the voltage, V_G , is producing the gain, G .

However, the PH resolution does not have such a simple multiplicative relationship with n_g . Because the avalanche variance generally decreases with increasing reduced field, two GEMs with unequal proportions of V_G will produce charge avalanches with different variances. This is a good reason to keep V_G divided roughly equally amongst the GEMs, as it should result in the lowest resolution for a given gain.

Pressure (torr)	Drift field (V/cm)	GEM field (kV/cm)	Collection field (V/cm)	V_1 (V)	V_2 (V)	$G_\infty = 100 \times a$	b (%)
20	283	19.1	1558	$(4.0 \pm 0.2) \times 10^2$	108 ± 6	n/a	34.5 ± 0.6
40	499	22.6	1842	$(6.2 \pm 0.2) \times 10^2$	84 ± 6	$(3.4 \pm 0.7) \times 10^4$	44 ± 5

Table 3: Pressures, field strengths, and fit parameters returned from Eqs. 9 and 13 characterizing the data, discussed in Section 4.2, recorded with an ^{55}Fe (5.9 keV) source in pure SF_6 using the 1-THGEM setup. Excluding the drift field, all fields values are some multiplicative factor of the total GEM voltage, V_G . The values shown here are associated with the highest V_G , i.e. highest gain, values of the data sets. The drift fields are held constant for all measurements where V_G is varied.

4. Measurements of gain and PH resolution

In this section we discuss gain and PH resolution measurements. Section 4.1 explains how gain and PH resolution are reconstructed from pulse-height data. In Sections 4.2 (SF_6) and 4.3 ($\text{He}:\text{CO}_2$) we present the measurements performed with the experimental structures pictured in Fig. 1 and the various GEM setups listed in Table 1. A discussion of the systematic issues can be found in Section 4.4.

4.1. Extracting the gain and PH resolution from data

The left panel of Fig. 3 shows a higher gain, approximately 6×10^4 (beyond the asymptotic gain value), $\text{He}:\text{CO}_2$ pulse-height spectrum recorded with the 3-t-GEM setup using an ^{55}Fe source. The center (20 torr) and right (40 torr) panels show typical SF_6 spectra, which present with consistently higher resolution when compared with the electron drift gas. These spectra are good examples of the data studied in this work, and can be used to illustrate the gain and PH resolution measurements.

The effective gain, G , is defined as the mean obtained from a χ^2 -minimization of a fit function to the pulse-height spectrum. The PH resolution is defined as the ratio of the standard deviation of the mean to the mean of the distribution, i.e. $R = \sigma_G/G$. All of the spectra are fit as a Gaussian distribution to the peak and exponential tails are used to amend any modified signal shape as needed, as not all of the distributions are symmetric, e.g. the left panel in Fig. 3

4.2. Measurements with SF_6 - a Negative Ion (NI) gas

As mentioned, Negative Ion (NI) gases have several potential advantages over traditional electron drift gases. However, NI gases are generally more difficult to work with because they require much higher reduced fields to produce gain as the electrons must be stripped away from the highly electronegative ions. In particular, SF_6 seems to suffer from large gain fluctuations and appears to be highly sensitive to impurities compared to CS_2 , which could be a disadvantage as NI gases are generally added to existing gas mixtures. These SF_6 measurements presented here are our group's first reported results with any NI gas.

4.2.1. The 1-THGEM setup

Fig. 3 shows pulse-height spectra from two SF_6 data sets, 20 torr (center) and 40 torr (right). These were both performed using an ^{55}Fe source with the 1-THGEM setup, and Fig. 4 shows the gain versus GEM voltage and PH resolution versus gain plots for these data sets.

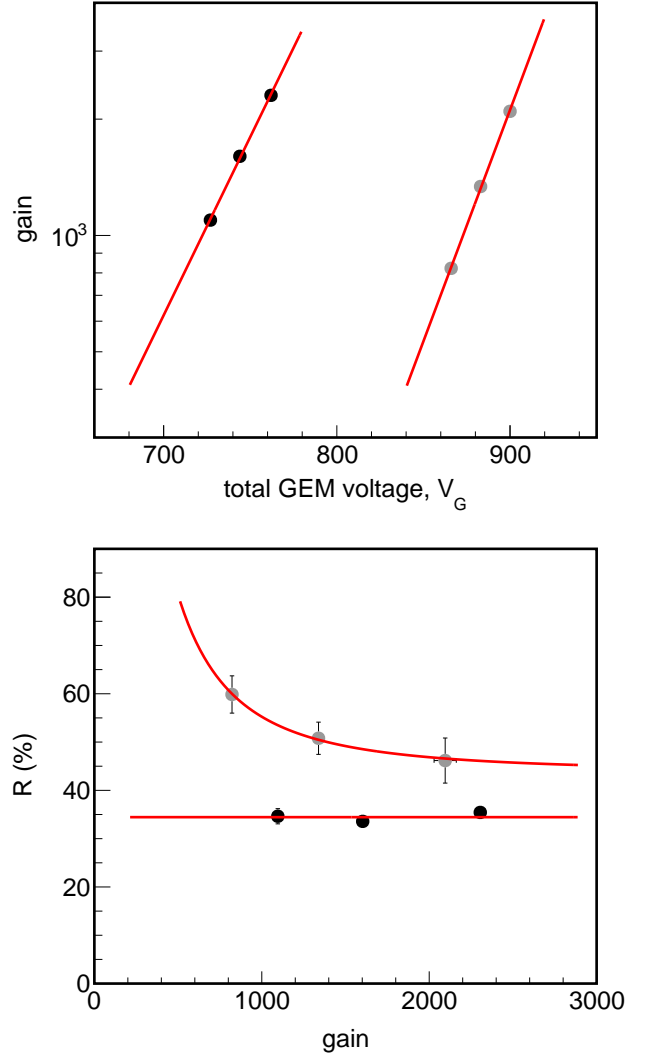


Figure 4: SF_6 data discussed in Section 4.2. Top: Gain versus total GEM voltage. Bottom: PH resolution versus gain. Data recorded with an ^{55}Fe (5.9 keV) source using the 1-THGEM setup at 20 torr (black points) and 40 torr (gray points). The solid lines (red online) are fits to the data of Eqs. 9 (top) and 13 (bottom).

As mentioned in the introduction, an electron must be stripped from the NI before it can initiate an avalanche. This is the reason that a higher reduced field is needed, and why these measurements are performed at low pressures. The effect of the material outgassing is more drastic at low pressures, and this was evident throughout these measurements. The result is

Setup	Pressure (torr)	Drift field (V/cm)	GEM field(s) 1:2:3 (kV/cm)	Transfer field(s) 1:2 (V/cm)	Collection field (V/cm)
2-tGEM	760	500	99.7 : 97.9	3853	3588
3-tGEM	760	509	74.0 : 75.1 : 74.9	1758 : 1706	2164
1-THGEM	380	239	26.5	n/a	2161
1-THGEM	570	291	33.0	n/a	2692
1-THGEM	760	469	37.3	n/a	3047
2-THGEM	760	500	32.6 : 31.0	2465	2211

Table 4: GEM setups and field strengths used for the gain and PH resolution measurements in ${}^4\text{He}:\text{CO}_2$ (70:30) using an ${}^{55}\text{Fe}$ source (5.9 keV) discussed in Section 4.3. Excluding the drift field, all fields values are some multiplicative factor of the total GEM voltage, V_G . The values shown here are associated with the highest V_G , i.e. highest gain, values of the data sets. The drift fields are held constant for all measurements where V_G is varied.

a substantial degradation of the gas gain over time, enough to affect a single five minute spectrum.

In order to combat this, constant gas flow was maintained at the maximum rate the system would allow, approximately 200 ml/min at 40 torr. This reduced the gain degradation to a few percent per hour. However, at 20 torr, the system could not maintain a high enough gas flow to completely offset the material outgassing, and this is evident in the top plot in Fig. 4. This shows that the slope of the gain versus V_G data recorded at 20 torr (black points) is less than that recorded at 40 torr (gray points).

The bottom plot in Fig. 4 shows the PH resolution versus gain. Notice that the 20 torr (black points) data is flat with the gain, which is another indication that the pulse-height spectra are not behaving as expected with varying V_G . Overall, the PH resolution seen here is worse than with an electron drift gas, such as He:CO₂. However, we note that the asymptotic resolution is lower for the higher reduced field (20 torr) measurements and this is summarized in Table 3. The behavior is expected as the avalanche should be lower at higher reduced fields.

Following the data recorded at 20 torr, measurements were performed at 30 torr and gain was also achieved at 60 torr. However, in both cases, the data quality was too low to assign a proper gain value. In summary, to achieve similar gain, SF₆ requires reduced fields up to an order of magnitude higher than with electron drift gases and the PH resolution is up to five times larger. However, collection and analysis of the full SF₆ waveforms could yield improvements to the PH resolution and provide further insight.

4.2.2. Other setups

SF₆ measurements were attempted with the other detector setups listed in Table 1 as well. However, for reasons that remain unclear, only the THGEMs produced positive results. This seems to run counter to the fact that SF₆ requires a high reduced field because thin GEMs can readily produce avalanching fields two to three times higher than THGEMs.

One explanation could be that a single THGEM produces more gain than a single thin GEM. A single 50 μm GEM produces gains of $\mathcal{O}(100)$, while a single 400 μm can produce gains of $\mathcal{O}(1000)$. This is why thin GEM setups usually consist of multiple GEMs and at least one transfer region. It is possible that the recombination in the transfer region renders the GEM

above it void for NI gases, and only the GEM closest to the collection plate is contributing to measurable gain. However, this does not explain why the same effect doesn't also occur in the collection region, between the last GEM surface and the collection plate. This warrants further study.

Gain was produced in the 2-THGEM setup, however the signal peak could not be fully resolved for assigning a proper gain value. One possible explanation is that only the final GEM is producing measurable gain because of recombination in the transfer region. The average field in the 2-THGEM setup is lower than in the 1-THGEM, so the signal from only one GEM producing gain in this case could lie below the noise floor.

4.3. Measurements with ${}^4\text{He}:\text{CO}_2$ (70:30)

He:CO₂, as discussed here is 70% ${}^4\text{He}$ and 30% CO₂. It is a safe, stable, electron drift gas that can achieve high gain. Given the similar masses of neutrons and the ${}^4\text{He}$ target nuclei, this gas is ideal for generating long recoil tracks induced from fast neutron collisions, and is the primary reason for its study here. It should be noted that, given the time span of these measurements, they were performed with two different bottles of gas, which were from the same vendor with the same specifications.

We will discuss six data sets from the four setups, and these details are summarized in Table 4. The results are shown in the plots in Fig. 5, which presents the gain versus total GEM voltage on the left and the PH resolution versus gain on the right for the six data sets. The following sections are in the order (top to bottom) of the plots shown in Fig. 5, which is also from the highest average reduced field in the GEMs to the lowest.

4.3.1. The 2-tGEM setup

The top row of Fig. 5 shows data recorded with the 2-tGEM setup, which was the final setup used. Owing to the experience obtained, and low material outgassing, this is some of the most stable data recorded. This is explicitly highlighted in Section 4.4.2 with Fig. 7. The data measured with the 2-tGEM setup was recorded at the end of a long stability run, in the gap on the right side of Fig. 7 where the resolution had degraded a bit from its minimum value. Gain values of $\mathcal{O}(10^4)$ and resolution values around 10% are typical with this and similar double thin GEM setups.

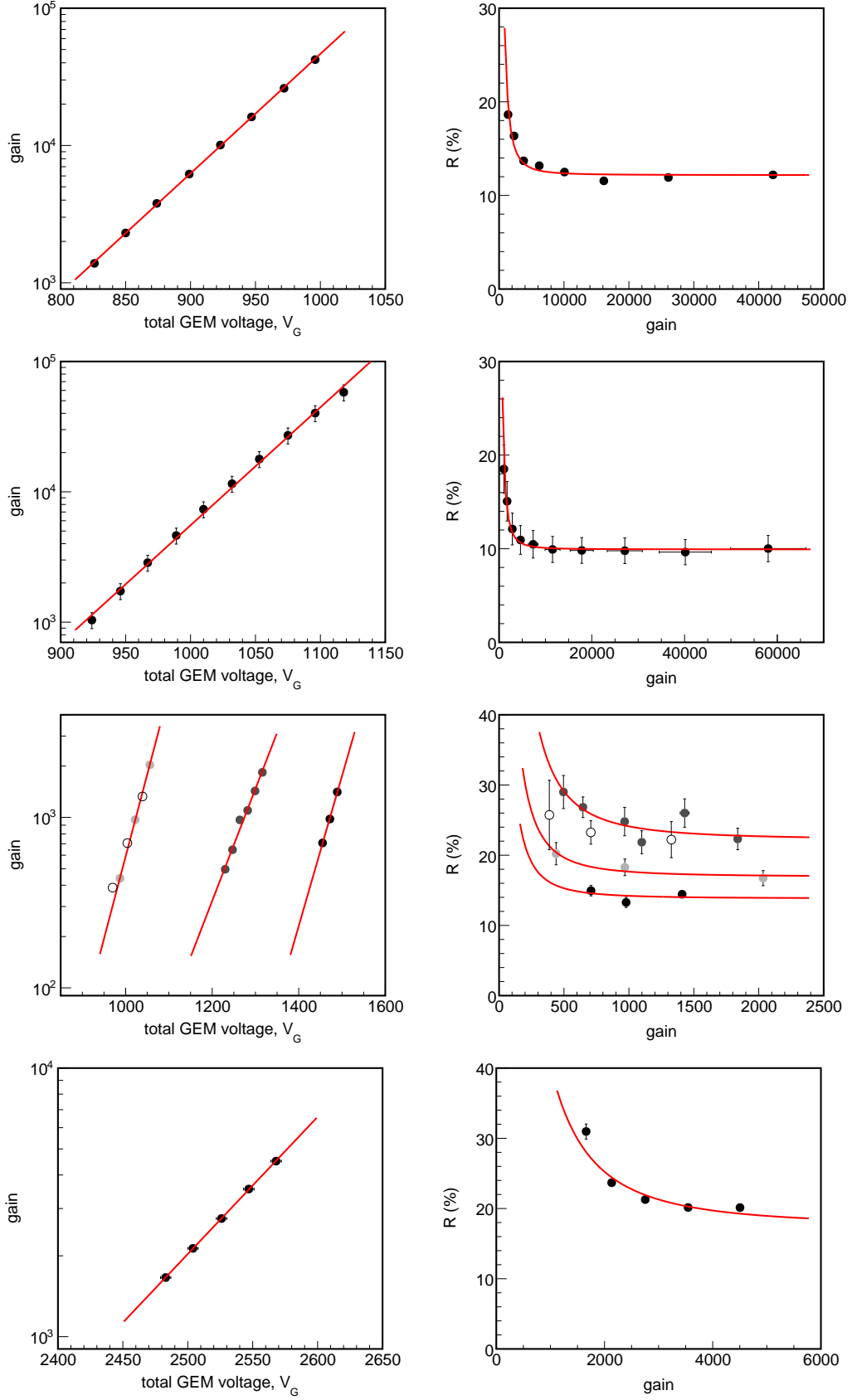


Figure 5: He:CO₂ (70:30) data obtained using an ⁵⁵Fe (5.9 keV) source discussed in Section 4.3. Top row: 2-tGEM setup. Second row: 3-tGEM setup. These error bars are due to calibration uncertainty as discussed in Section 2.4. Third row: 1-THGEM setup, from left to right: 380 torr (light gray points, open circles are not included in fits), 570 torr (dark gray points), and 760 torr (black points). Last row: 2-THGEM setup. The solid lines (red online) are fits to the data of Eqs. 9 (gain versus the total GEM voltage, left) and 13 (PH resolution versus gain, right).

Setup	Pressure (torr)	Reduced GEM field(s) 1:2:3 (V/cm/torr)	V_1 (V)	V_2 (V)	$G_\infty = 100 \times a$	b (%)
2-tGEM	760	131 : 129	463 ± 4	115 ± 1	$(2.15 \pm 0.05) \times 10^4$	12.17 ± 0.09
3-tGEM	760	97 : 99 : 99	$(5.9 \pm 0.1) \times 10^2$	110 ± 4	$(1.8 \pm 0.3) \times 10^4$	9.9 ± 0.5
1-THGEM	380	70	$(7.1 \pm 0.1) \times 10^2$	104 ± 4	$(5 \pm 2) \times 10^3$	16.9 ± 0.9
1-THGEM	570	58	$(8.2 \pm 0.2) \times 10^2$	152 ± 5	$(9 \pm 2) \times 10^3$	22 ± 1
1-THGEM	760	49	$(1.13 \pm 0.3) \times 10^3$	$(1.1 \pm 0.1) \times 10^2$	$(3 \pm 3) \times 10^3$	13.8 ± 0.8
2-THGEM	760	43 : 41	$(1.86 \pm 0.4) \times 10^3$	$(2.0 \pm 0.1) \times 10^2$	$(3.6 \pm 0.2) \times 10^4$	17.5 ± 0.5

Table 5: Experimental setup names, pressures, and fit parameters returned from Eqs. 9 and 13 characterizing the data, discussed in Section 4.3, obtained with an ^{55}Fe (5.9 keV) source in $^4\text{He}:\text{CO}_2$ (70:30). From the top row going down the reduced GEM field, which is shown for the highest gain value in each data set, decreases and the variance of the avalanche distribution should increase as this happens. If all other effects are accounted for this will correspondingly increase the asymptotic PH resolution, b . The values shown here are before any stability corrections are applied, however one can see the average b value at 760 torr for the 2-tGEM and 3-tGEM setups is lower than that for the 1-THGEM and 2-THGEM setups.

4.3.2. The 3-tGEM setup

The second row from the top in Fig. 5 shows the measurements obtained with the 3-tGEM setup. As mentioned in Section 2.4, the error bars in these two plots are larger due to the larger calibration uncertainty. This data set was also recorded at the end of a long stability run. However, the setup used here (Fig. 1 left) consists of more material which increases outgassing, and this results in larger degradation of the gain and resolution over time. One way to reverse the degradation is to flow gas through the vessel until the gain recovers, and this was done preceding this data set. This is evident in the slight ‘bend’ in the gain versus V_G data, i.e. the highest and lowest gain data points both fall slightly below the solid line of best fit. Although the gas flowed had been stopped by the time of measurement, this suggests the gain was still slightly in flux from the procedure.

We note that gain values of $O(10^4)$ and resolution values around 10% are typical with this setup as well. While, the 2-tGEM setup does produce a slightly higher asymptotic resolution value of approximately 13%, this is before the signal degradation over time has been taken into account. It’s also important that the asymptotic resolution for the 3-tGEM setup was recorded immediately after substantial gas flow. We will see that once the changes over time, i.e. stability, is taken into account, these values are much closer to one another. This suggests that the number of thin GEMs, and hence the number of transfer regions, has little effect on the PH resolution. However, this is not the case for the THGEM setups.

4.3.3. The 1-THGEM setup

The third row from the top in Fig. 5 shows the measurements obtained with the 1-THGEM setup. Data was recorded at three different gas pressures, 380 (light gray points), 570 (dark gray points), and 760 torr (black points). The first thing to notice is the obvious lower gain and worse resolution when compared with the data from thin GEMs. This can be expected as THGEMs typically operate at lower reduced fields.

The 380 and 570 torr data sets were recorded during the same time period, and this is the reason for the larger fluctuations. A long stability run was performed at 380 torr followed by the recording of the first three data points in Fig. 5 (closed light

gray circles). The pressure was then increased and the entire 570 torr data set was recorded. After this, the pressure was lowered back down to 380 torr and the remaining three data points (open light gray circles) were recorded. This is the reason that the 380 torr data, especially the resolution versus gain, is noticeably split into two different groupings. Only the closed circles are fit with Eq. 9 and Eq. 13 and included in the subsequent analysis.

We also note that 570 torr data is affected by the absence of a long stability run and being recorded in close proximity to a change in pressure. Specifically, the slope of the gain versus V_G data slightly lower than expected, and the resolution is substantially higher. It is not included in any further analysis and we include it here for completeness. Following the measurements at 380 and 570 torr, the chamber was evacuated and then filled to atmospheric pressure. After a period of stabilization, the data at 760 torr was recorded.

Finally, the most notable issue with the 1-THGEM setup was that it produced the lowest overall SNR, achieving maximum gains of $O(1000)$. In fact, the grounding scheme used with the thin GEM setups had to be improved before any gain from a THGEM could be measured, and being closer to the noise floor resulted in some non-Gaussian spectra features. As mentioned, exponential tails were included in the fitting functions as needed but, in the future, collecting and analyzing the full waveforms could be beneficial.

4.3.4. The 2-THGEM setup

The bottom row in Fig. 5 shows the measurements obtained with the 2-THGEM setup, and there are two things to note. First, although stable gain was achieved, the amount of voltage required was high and sparking was a major issue. Compared to the 1-THGEM setup, the gain was more stable and uniform with a higher SNR resulting in gains of several thousand. A redesign of this system to reduce the sparking would likely prove fruitful.

Second, the asymptotic PH resolution is substantially worse for the 2-THGEM setup than for the 1-THGEM at the same gas pressure. Naively, it is not obvious that this should be the case but Eq. 16 offers an explanation. However, we must first account for the systematic differences between the setups, and

specifically the stability of the gain and resolution over time.

4.4. Measurements of systematics with the 2-tGEM setup

The measurements discussed throughout this work spanned multiple years and experimental setups. A concerted effort was taken to account for, and minimize, systematic issues. Most of the typical systematic differences between setups result in multiplicative constants affecting the gain. This translates into the gain versus V_G relationships from different setups, which are plotted with logarithmic vertical axes, retaining their shapes, but being shifted vertically relative to one another. However, issues concerning gas purity, i.e. cases where gas flow was required for stable gain, or instances where different gas bottles were used, can affect the relative gain difference within a given setup or data set. This will alter the slope of the gain versus V_G relationship and is difficult to account for.

There are many parameters that can affect gas gain. With GEMs, the mechanical design is an important consideration for suppressing discharges and allowing for seamless integration, but can also impact the gain. The hole geometry and the insulating material, which can charge up, will both have effects. There is also the issue of electric field line continuity between the different regions, above and below the GEM(s). If many of the field lines have undesired terminations, then the measured gain can be substantially degraded. Here, we choose the maximum transfer and collection field values that are stable but optimize no further.

For completeness, we summarize the various systematic uncertainties. We mention again the approximately 14% uncertainty on the system response value for the 3-tGEM setup. This directly translates into an uncertainty on the gain values, and is included throughout Sections 4.3 and 5.3 as it impacts the uncertainty on most of the fit parameters. Given the calibration procedure for the resistive dividers used, there is an approximately 0.16% uncertainty on all voltage values. Pressure values have an uncertainty of 1%, with the exception of those used in SF₆, which are estimated at 2% to account for the gas flow that had to be maintained. The uncertainty in the GEM thickness is estimated to be 1%, and all of these values are included within the error bars and quoted uncertainties throughout. In what follows, we will discuss dedicated data sets recorded to study the effect of the drift field and the system stability. For both studies, the stable 2-tGEM setup was used with an ⁵⁵Fe source in He:CO₂ at atmospheric pressure.

4.4.1. Drift field

Present in all setups is the effect that the drift field strength has on the gain and PH resolution. Essentially, when the transport of charge to the GEMs becomes most efficient the gain and PH resolution will reach a plateau. For this study, V_G was held constant at 874 V which corresponds to a gain of approximately 4000. This is the same setting as used for the third data point from the left in the top left plot in Fig. 5.

Fig. 6 shows both the gain (top) and PH resolution (bottom) versus the drift field, E_{drift} . As expected, both plateau at a certain value of E_{drift} . We introduce

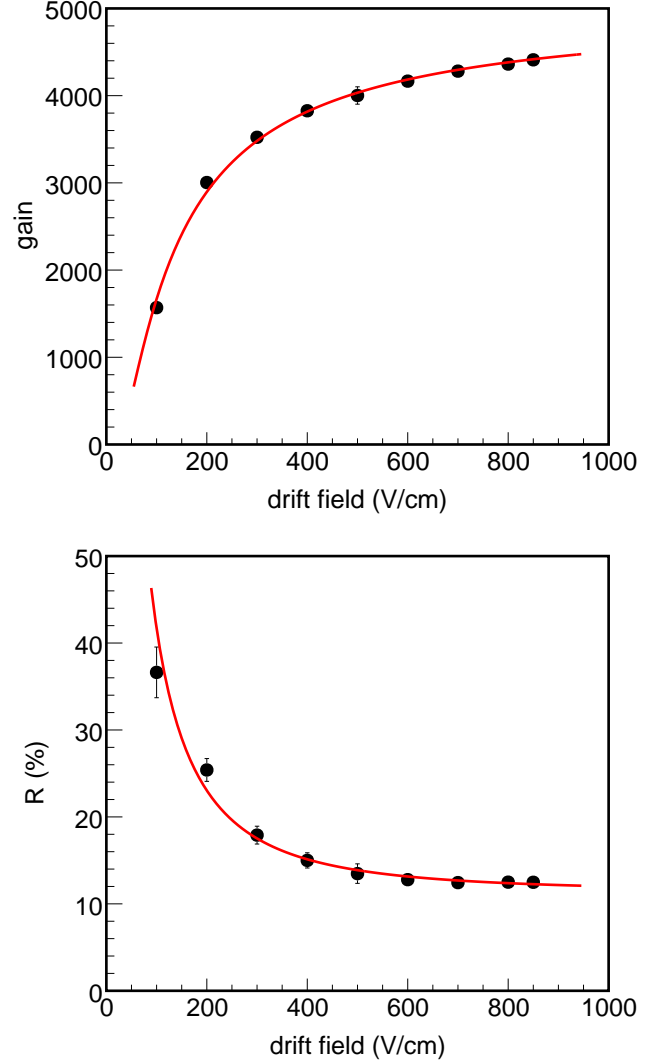


Figure 6: He:CO₂ data discussed in Section 4.4.1 obtained with an ⁵⁵Fe (5.9 keV) using the 2-tGEM setup at atmospheric pressure. Top: Gain versus drift field. Bottom: PH resolution versus drift field. The solid lines (red online) are fits to the data of Eqs. 19 (top) and 20 (bottom).

$$G = 10^{c - E_1/E_{drift}}, \quad (19)$$

to describe the gain as a function of E_{drift} and

$$R = \sqrt{\left(\frac{e}{E_{drift}}\right)^2 + d^2}, \quad (20)$$

to describe the PH resolution as a function of E_{drift} .

The solid lines in Fig. 6 are fits to the data points of Eqs. 19 (top) and 20 (bottom). The extracted parameters are listed in Table 6 and we will briefly comment on them. At infinite drift field, c is the log of the gain. E_1 is the drift field value at which the gain is approximately 10% of its asymptotic value. As in Eq. 13, d is the asymptotic fractional PH resolution at high drift field in this case. e is the value of drift field below

c	E_1 (V/cm)	e (V/cm)	d (%)
3.70 ± 0.01	48 ± 2	40 ± 2	11.3 ± 0.4

Table 6: Fit parameters, defined by Eqs. 19 and 20, characterizing the gain and PH resolution versus drift field data recorded with an ^{55}Fe (5.9 keV) source in $^4\text{He}:\text{CO}_2$ (70:30) using the 2-tGEM setup at atmospheric pressure discussed in Section 4.4.1

which the sigma of the pulse-height is certain to be greater than the mean. With the exception of the middle data points, all gain and PH resolution values in Fig. 6 are obtained from a single five minute spectrum, and the error bars arise from fitting the distribution. However, the middle points are the result of the average of multiple five minute spectra, and these error bars highlight the stability of this setup over roughly the timespan of this set of stability measurements.

We use this data set to point out that all of the atmospheric pressure He:CO₂ measurements in Section 4.3 were recorded with a drift field of approximately 500 V/cm. As evident in Fig. 6, this is not the optimal drift field for maximizing the gain or minimizing the PH resolution. However, measured at a drift field of 500 V/cm, the PH resolution is within a few percent of its asymptotic value and any previous conclusions will be minimally affected by this. Nonetheless, operating at a high enough drift field to achieve certain detector performance metrics is an important design consideration.

4.4.2. Stability

Many factors can affect gas gain and PH resolution stability including temperature, gas purity, and devices charging up. In this work, an intense effort was undertaken to understand the stability for all of the setups discussed. Usually, the stability was monitored for days before and after our primary measurements of varying V_G were recorded and we can note a few general features.

Immediately following the initial fill of the vacuum vessel there is always a ‘stabilization’ period, where the gain increases a few percent before reaching a plateau. The exact mechanism of the gain increasing after the initial back-fill is not obvious, although it does seem to be related to the gas itself as opposed to an electronics or readout issue. The rapidly expanding gas is cold and will warm up after filling into the vessel. However, if the initial gain variation were related to the gas temperature, one would instead expect the gain to decrease as it goes as the inverse of pressure. Whatever the case, this period lasts for up to 30 minutes after which the gain becomes stable.

If neither a gas purification system nor gas flow is used, gas gain will degrade over time. The degree of the degradation and the timeline involved can depend on many factors, but the largest culprit is the outgassing of the detector components. In the setups with low material outgassing, including the 2-tGEM setup, the gain with atmospheric pressure electron drift gases can remain stable within a few percent for many days. We recall that the gain is proportional to the mean of the pulse-height distribution and this will decrease along with the gas purity, while the sigma of the distribution increases. A commonly observed

feature is that the sigma degrades more dramatically, roughly three to five times, compared to the mean. As a result, the PH resolution is much more sensitive to gas purity issues than the gain itself.

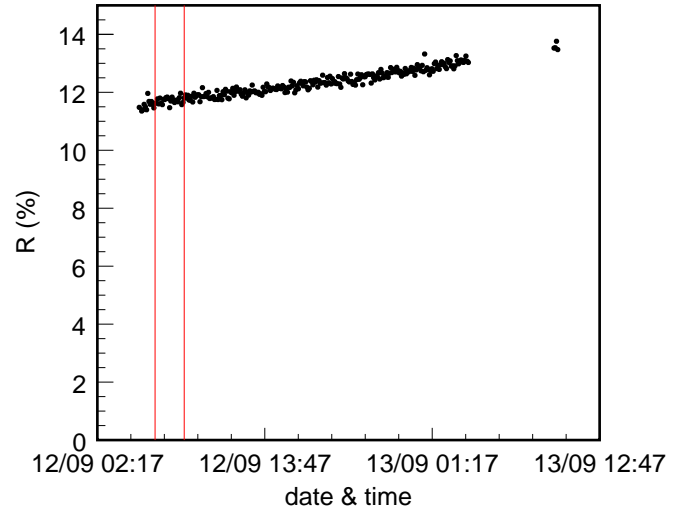


Figure 7: He:CO₂ (70:30) resolution stability data discussed in Section 4.3 obtained with an ^{55}Fe (5.9 keV) source using the 2-tGEM setup at atmospheric pressure. The solid vertical lines (red online) enclose the two hour time period used for correcting the resolution against degradation over time, which is applied and discussed in Section 5.3.3.

Fig. 7 shows the fractional PH resolution stability of the 2-tGEM setup. Over this time period the sigma of the signal distributions increased by approximately 10%, while the means decreased by only a few percent. The gap on the right indicates the time during which the measurements discussed in Section 4.3.1 were performed. We note that the PH resolution during this time is a few percent higher than near the beginning of the stability run. As the PH resolution can change substantially over time, we will use this stability run, along with runs associated with the other setups, in Section 5.3.3 to obtain a minimum value for the energy resolution in GEM-based detectors.

5. Further analysis using reduced quantities

We will now present the data in a more comprehensive way. Using the remaining ideas introduced in Section 3, we will analyze the dependence of the Reduced First Townsend Coefficient on the reduced field (i.e. RFTC versus Σ). This is essentially a generalization of the more commonly considered dependence of gain on the total GEM voltage (i.e. G versus V_G). In Section 5.1, we revisit some earlier Ar:CO₂ (70:30) data [6]. We show that gas gain data with vastly different initial ionization energies can be described using a single functional form. In Section 5.2, we discuss the SF₆ data. Finally, in Section 5.3, the richer He:CO₂ data sets are used to illustrate all of the gain and resolution concepts presented in Section 3.

With all three gases, we are comparing the performance of Eq. 10, where $m = 1$, and Eq. 8 with $m = 0$. Setting $m = 0$ in Eq. 8 is deliberate as there is not enough data to properly

constrain this parameter, and the results are summarized in Table 7. Further studies focused on keeping systematic uncertainties low could yield more insight about the behavior of m , and whether it changes with different gas mixtures. Recall that m is a measure of how dependent the cross section of interaction between an accelerating electron and an atomically bound electron is on the reduced field, and $m = 0$ implies that the cross section is independent of the reduced field. We also note that, while the physical interpretations of the parameters A and B in Eq. 8 are obscure, the value of B/A can be regarded as a measurement of the ionization potential of the gas mixture [25, 33]. The W-values that were used in determining the gain values are provided for comparison where appropriate.

5.1. Reduced quantities across different ionization energies in Ar:CO₂ (70:30)

In Ref. [6] a double-thin-GEM detector, similar to the 2-tGEM setup used here, was used to measure gas gain in Ar:CO₂ (70:30). Both ⁵⁵Fe (5.9 keV X-rays) and ²¹⁰Po (5.3 MeV α -particles) were measured. Due to the lack of precise information about the ²¹⁰Po source location with respect to the sensitive volume, the measured ionization energy from the α -particles was estimated to be approximately 4 MeV with a large uncertainty. The spectra associated with the α -particles were integrated for 30 minutes, as the rate is much lower than that of the ⁵⁵Fe source.

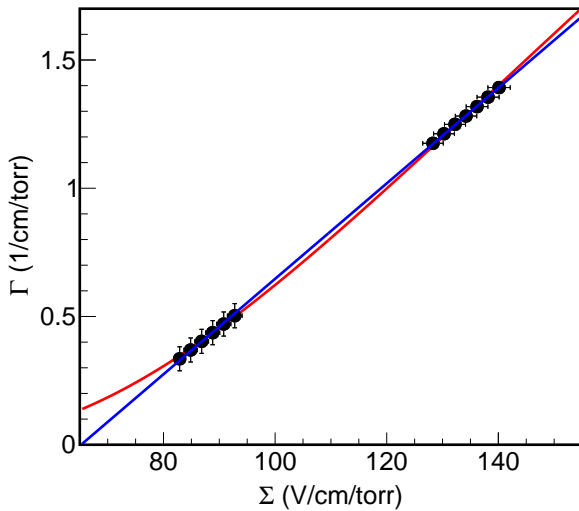


Figure 8: Reduced First Townsend Coefficient (RFTC) versus reduced field for the Ar:CO₂ (70:30) data discussed in Section 5.1. Data recorded with two different energy sources, approximately 4 MeV collected with alpha particles from ²¹⁰Po (left grouping) and 5.9 keV X-rays from ⁵⁵Fe (right grouping), using a double-thin-GEM detector setup at atmospheric pressure described in Ref. [6]. The solid lines are fits to the data of Eq. 10 (blue online) and Eq. 8 with $m = 0$ (red online).

Fig. 8 shows the RFTC versus the reduced field for the two different ionization energies measured in Ar:CO₂ at atmospheric pressure. The group of data points on the left is from the α -particles, which produce roughly three orders of magnitude more ionization than the 5.9 keV X-rays (group of points

on the right). The result is that a much lower gain is required to measure the ionization produced by the α -particles. The solid lines are fits of Eq. 10 (blue online) and Eq. 8 with $m = 0$ (red online). For reference, a W-value of 28.05 eV [34] was used to determine the gain values measured in Ar:CO₂ discussed in Ref. [6]. It should also be mentioned that the electric fields in the transfer and collection regions are approximately 40% lower for the α -particle measurements than for the 5.9 keV X-rays. This is because these fields are proportional to the GEM fields, which are lower for the α -particle measurements. This could be introducing some inefficiencies which is resulting in lower measured gain than compared to if these fields were held to the same values as in the ⁵⁵Fe measurements.

Regarding the PH resolution, as evident in Eq. 18 the asymptotic PH resolution will decrease with the square root of the initial ionization energy. This is discussed more in Refs. [6] and [15]. Over the range of reduced field considered here, the avalanche variance does change and is likely quite large for the low gain values associated with the α -particle measurements. In further analyses involving the PH resolution values obtained with vastly different ionization energies, this change in the avalanche variance should be taken into account along with any changes in the ionization energy and resulting changes of the Fano factor.

5.2. Reduced quantities in SF₆

SF₆ lives in a different part of the parameter space when compared to the electron drift gases, operating at higher reduced fields and achieving higher RFTCs. Fig. 9 shows the RFTC versus the reduced field for the two SF₆ data sets, recorded with the 1-THGEM setup at 20 and 40 torr. The solid lines are fits of Eq. 10 (blue online) and Eq. 8 with $m = 0$ (red online) to the reduced quantities. For reference, a W-value of 34 eV [35] was used to determine the gain values for SF₆ shown in Fig. 4.

Both equations provide an adequate description of the range of RFTC as a function of reduced field, however the slopes of the individual data sets are steeper than predicted by either equation. This effect is observed with the larger He:CO₂ data sets as well and is explored further in Section 5.3.1. Here we note that neither Eq. 10 or Eq. 8 account for any charge loss effects, e.g. the complicated inelastic and recombination processes, present inside of a real detector. These effects are exacerbated with a NI gas like SF₆. This is studied in some detail in Ref. [36] but, briefly, NI gases produce charge avalanches in the same way that electron drift gases do, by accelerating electrons causing ionizing collisions with other, atomically-bound, electrons. The difference is that the initiating electron must first be stripped from the NI. This process is complicated by the variance in the energy required to strip the electron, and by the existence of various NI species with different attachment coefficients. In addition, when compared with any electron drift gas mixture, more recombination takes place during the avalanche itself which will lead to even more variance in the final pulse.

5.3. Asymptotic, reduced quantities in ⁴He:CO₂ (70:30)

We will now discuss the He:CO₂ data within the more formal language of Section 3. As mentioned in Section 4.3.3, this is a

Gas (fit to which quantities)	Fit with Eq.	χ^2	ndf	$1 - P$	B/A (V)	Σ_1 (V/cm/torr)	V_3 (V)
Ar:CO ₂ (all reduced)	10	0.079	11	6.5×10^{-11}	n/a	65 ± 2	54 ± 2
Ar:CO ₂ (all reduced)	8 ($m = 0$)	0.326	11	1.4×10^{-7}	27 ± 3	n/a	n/a
SF ₆ (all reduced)	10	2.142	4	0.290	n/a	$(2.0 \pm 0.2) \times 10^2$	80 ± 4
SF ₆ (all reduced)	8 ($m = 0$)	2.176	4	0.297	37 ± 3	n/a	n/a
He:CO ₂ (asymptotic)	10	0.274	3	0.035	n/a	33 ± 1	71 ± 2
He:CO ₂ (asymptotic)	8 ($m = 0$)	0.256	3	0.032	35 ± 2	n/a	n/a

Table 7: Summary of parameters extracted from fitting Eqs. 8 and 10 to the reduced quantities in Figs. 8 (Ar:CO₂) and 9 (SF₆), and the asymptotic, reduced quantities for He:CO₂ in the top plot of Fig. 10. Here, the value $1 - P$ is the probability that the χ^2 value from a random model would be less than the quoted result, so a lower value reflects a better description of the data. Notice that both equations describe the asymptotic, reduced quantities nearly equally well. We fix $m = 0$ in Eq. 8, as there is not enough data to properly constrain it.

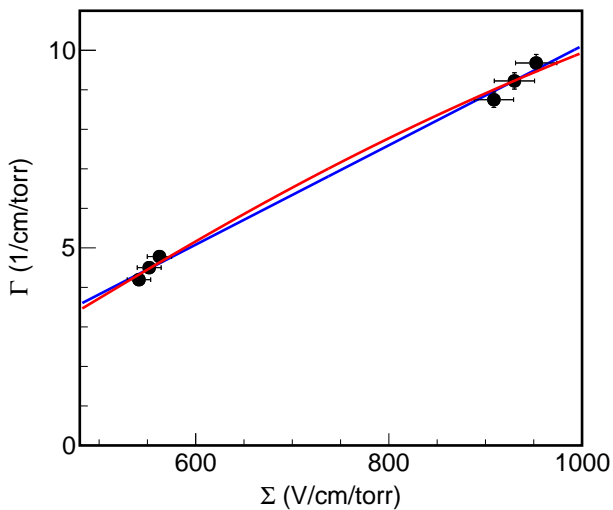


Figure 9: Reduced First Townsend Coefficient (RFTC) versus reduced field for the SF₆ data discussed in Section 5.2. Data recorded with an ⁵⁵Fe (5.9 keV) source using the 1-THGEM setup at two different pressures, 40 torr (left grouping) and 20 torr (right grouping). The solid lines are fits to the data of Eq. 10 (blue online) and Eq. 8 with $m = 0$ (red online).

subset of the data discussed in Section 4.3. We exclude some of the 380 torr data along with the 570 torr data set. The motivation for this section begins by considering all of the plots in Fig. 5 together and looking for an obvious relationship between the gain and the energy resolution. This eventually leads to the consideration of the asymptotic reduced quantities which allow us to understand the gain and energy resolution in GEM-based detectors in a broader context.

5.3.1. The asymptotic RFTC versus the asymptotic reduced field

The top plot in Fig. 10 shows the asymptotic RFTC versus the asymptotic reduced field, as defined in Eq. 15. Note that each of the five data sets is described by a single value. The solid lines are fits to the asymptotic reduced quantities from Eq. 10 (blue online) and Eq. 8 with $m = 0$ (red online). For reference, a W-value of 34.4 eV [34] was used to determine the gain values for He:CO₂ shown in Fig. 5.

While constraining m is not possible here, we can note a few

implications. If $m = 1$, then α is strictly proportional to the avalanching field strength in the GEM. From this follows the strictly exponential dependence of the gain on V_G for a given setup at a given pressure. If $m \neq 1$, there will be a deviation from this strictly exponential dependence of the gain on V_G . These deviations are not drastic within the reduced field range where GEM-based detectors typically operate, and a range of values for m provide adequate descriptions of the data. However, another outcome of $m = 1$ is that the gain is predicted to increase without bound, whereas $m \neq 1$ indicates that the gain will indeed approach a limit. This is expected and will continue as recombination effects increase and space charge issues arise until the Raether limit [37] is reached.

The bottom plot in Fig. 10 shows all of the RFTC values versus the reduced field values for the five He:CO₂ data sets. The solid lines are overlays of the fitted lines from the top plot to show where the models fall within the full data sets. Recall that the definition of the asymptotic gain is $100 \times a$, where a is the noise parameter obtained from fitting the PH resolution versus gain data. If a is larger for one setup, the corresponding asymptotic quantities will be as well and this will cause the models to lie slightly above the measured data. Also, if a slightly smaller then the models will fall below the measured data.

Equation 8 is certainly a better physical model than Eq. 10, but it is still simple and neglects many effects present in a real detector. For one, not all electrons with energy above the ionization potential of the gas will necessarily produce an avalanche, and no inelastic effects are considered. And, because nearly all effects that are unaccounted for will produce a loss of electrons, both models will generally predict a higher gain than will be measured in a real detector.

In the end, both Eqs. 10 and 8 with $m = 0$ can describe the high-gain behavior of all detectors well, in a unified way. This is in the limit where detector noise is not affecting the measurements, and illustrated in the top plot in Fig. 10. However, the bottom plot shows that the lower-gain behavior of each detector cannot be described with the same models. The lower-gain points are presumably affected by effects that are not included in the models, including detector noise, gas impurities, and other charge-loss mechanisms.

In fact, if the observed gain values are underestimates, and the true gain values are closer to the model predictions, this

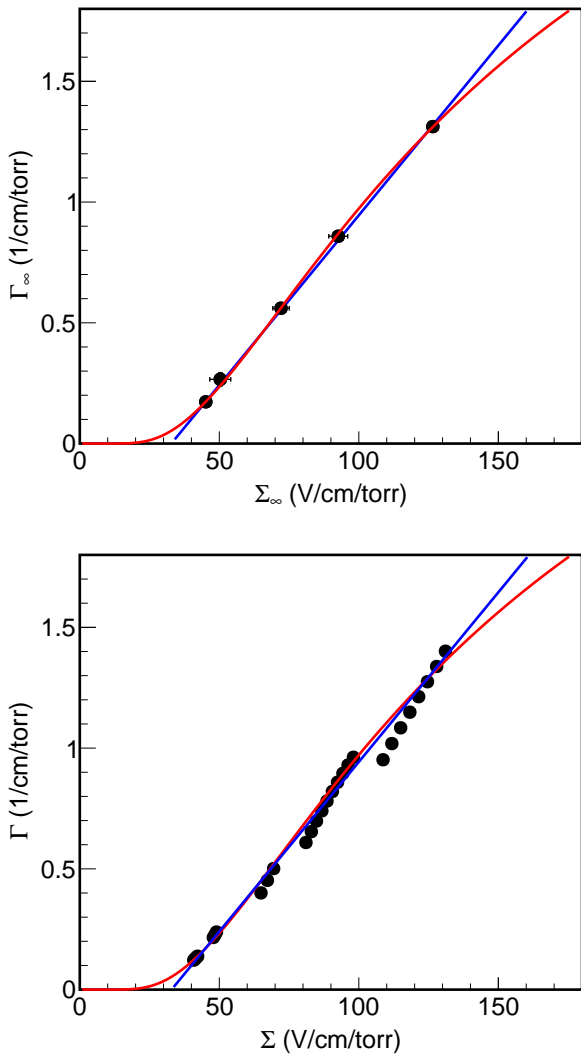


Figure 10: Top: Asymptotic Reduced First Townsend Coefficient (asymptotic RFTC) versus asymptotic reduced field. Bottom: Reduced First Townsend Coefficient (RFTC) versus reduced field. He:CO₂ (70:30) data. For reasons discussed in Section 4.3.3, this is a subset of the data shown in Fig. 5. In the top plot, the solid lines are fits to the data of Eq. 10 (blue online) and Eq. 8 with $m = 0$ (red online).

would also cause the PH resolution values at lower gain to decrease, assuming the sigmas remained constant. This would result in the PH resolution versus gain data to ‘flatten’ towards lower gains, and would be consistent with what has been observed in a similar GEM-based detector with a highly segmented, low-noise, pixel ASIC readout [7]. So, this large noise term from the charge collection plate and analog readout electronics could be causing multiple issues at low gain.

Whatever the case, fitting Eq. 8 to the asymptotic reduced values across a broad range of parameter space, as done in the top plot of Fig. 10, will return more accurate values for the gas-dependent parameters A and B than using only the values from any individual setup. Again, it is not clear from this analysis that m could ever be constrained via this method, but it would be interesting to pursue this further with a focus on minimizing

the systematic issues. We also reiterate the benefit of Eq. 8, whatever the value of m , over the threshold model, Eq. 10, which is certainly more unphysical.

We should also point out the robust nature of the proportional relationship between Γ_∞ and Σ_∞ , and to some extent between Γ and Σ as well. Recall that the RFTC is measurement of the number of electrons per unit length per unit pressure being produced in the avalanche. So, for a given gain and gas pressure, this number will decrease with increasing GEM thickness. For instance, a slightly thicker GEM with specific hole geometry may produce more gain at a lower reduced field than another GEM with a different hole geometry than only the avalanching field strength difference can explain. However, even though the gain may be larger for the thicker GEM, the RFTC will be less affected and possibly have smaller value. This effect is due the logarithm of the gain in the numerator and the GEM thickness in the denominator of the RFTC. This illustrates that effects like GEM material or geometry play a much less significant role in determining the RFTC value than the reduced field.

5.3.2. Relating the variance of the avalanche distribution to the asymptotic reduced field via the χ parameter

A general feature for many models of charge avalanches within uniform electric fields is that the variance will decrease as the reduced field increases. Since this variance is a large contributor to the PH resolution, we would expect the same behavior from it. Continuing the discussion about the parameter χ will help lead us there.

Eq. 11 shows that χ is proportional to the RFTC divided by the reduced field. The constant of proportionality is a model parameter that represents the ionization potential of the gas. Here, the returned value of B/A listed in Table 7 is used. However, we are not as interested in the value of χ as we are in its functional dependence on the reduced field. The reason is that the variance of the avalanche distribution will decrease and reach a minimum value as χ increases to reach a maximum [30].

Fig. 11 shows the χ values versus the asymptotic reduced field. The solid line is a fit of Eq. 12 to the data points where A , B , and m are fixed to their values returned from fitting Eq. 8 with $m = 0$ to the asymptotic reduced quantities in the top plot of Fig. 10, and only a scale factor is left as a free parameter. The maximum χ value occurs at approximately 143 V/cm/torr for this gas, indicating that this is where the avalanche variance will reach its minimum value.

More specifically, what is shown in Ref. [30] is that for Legler’s and other models the variance of the avalanche distribution has a complicated dependence on χ . One reason for this is because, as the avalanching field increases, the avalanche distribution changes [29] from exponential to something closer to a Polya distribution, which is peaked near the mean multiplication factor and has a lower variance. However, in addition to decreasing toward a minimum as χ increases towards a maximum, the avalanche variance changes more at lower values of χ than it does near its minimum. This translates into the following: If the only remaining gain, or reduced field, dependent term that is contributing to the PH resolution is the avalanche variance, then at lower reduced field values the PH resolution

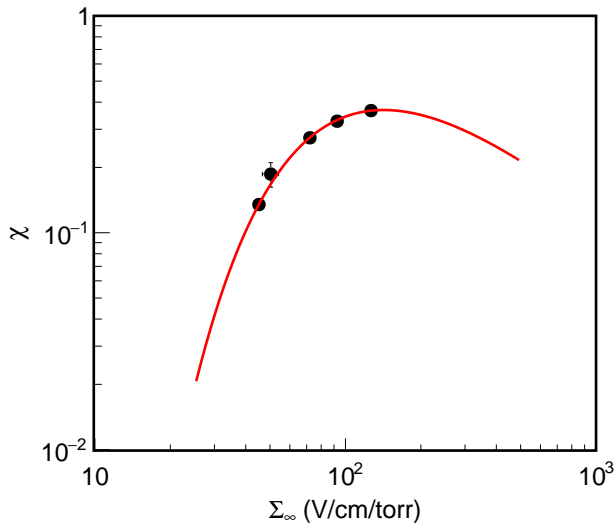


Figure 11: χ versus the asymptotic reduced field for the He:CO₂ (70:30) data. For reasons discussed in Section 4.3.3, this is a subset of the data shown in Fig. 5. The solid line (red online) is a fit to the data of Eq. 12. The minimum value of the avalanche distribution variance should occur at the maximum value of χ .

will change more than at higher values near the maximum χ value.

5.3.3. The asymptotic PH resolution versus the asymptotic RFTC

Our discussion about χ allows us to determine at what reduced field value the minimum avalanche variance value, and hence the minimum PH resolution, should occur but it doesn't yet tell us anything about its actual value. To proceed, after applying corrections to the PH resolution from the stability data, we will return to the end of Section 3.2.2 and Eq. 16 for a final word about the minimum obtainable energy resolution in GEM-based detectors.

As mentioned in Section 4.4.2, in an effort to obtain an accurate value for the minimum energy resolution in GEM-based detectors, we use the stability data obtained with the detector setups to correct the PH resolution values. We define a two hour period bounded by the two vertical red lines in Fig. 7 that follows the stabilization period discussed earlier in Section 4.4.2. This is when the gain is stable and the resolution is nearest its minimal value for a particular setup. The procedure follows.

We average the values obtained from all of the five minute spectra within the two hour period. We then take the difference between said average value and the measured values shown on the right of Fig. 5. This difference is then subtracted from the values in Fig. 5. This results in PH resolution values that would have been obtained had the data set been measured earlier in the stability run. The analysis is then re-run and corrected asymptotic PH resolutions values are obtained, and these are denoted as R_{∞}^* . We note that some of the data sets were recorded near the beginning of stability runs, so this procedure is only performed where appropriate.

Fig. 12 shows the corrected asymptotic PH resolution versus the asymptotic RFTC. The solid line is a result of fitting Eq. 16

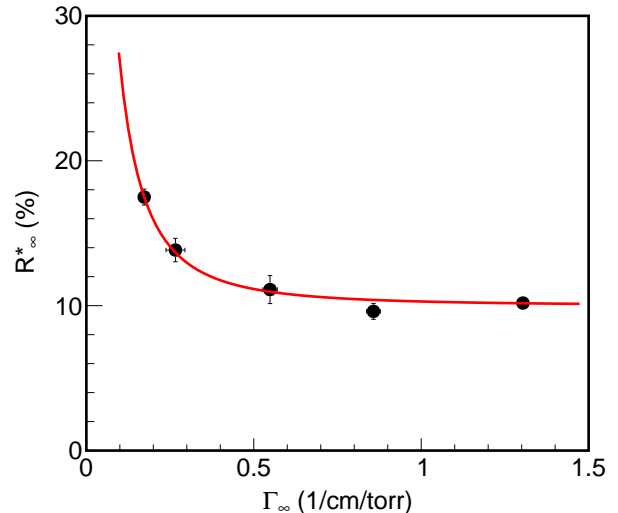


Figure 12: Asymptotic PH resolution versus the asymptotic RFTC for the He:CO₂ (70:30) data. For reasons discussed in Section 4.3.3, this is a subset of the data shown in Fig. 5. The solid line (red online) is a fit to the data of Eq. 16. The asymptotic value approached in this figure can be regarded as a minimum of the achievable energy resolution at a given ionization energy for a given gas mixture in GEM-based detectors.

to the data points. The values obtained for \mathcal{A} and \mathcal{B} are $(2.5 \pm 0.1) \times 10^{-2}$ 1/cm/torr and $(9.98 \pm 0.09)\%$, respectively, and \mathcal{B} can be interpreted as the minimum achievable energy resolution for this gas with this initial ionization energy, 5.9 keV.

This can be taken one step further by recalling that the drift field is not optimized to minimize the PH resolution in this data. This was explicitly shown in Section 4.4. All of the asymptotic PH resolution values here could presumably be lowered by approximately 2% if these measurements were performed at a higher drift field, and doing so would shift the value of \mathcal{B} down to approximately 8% at 5.9 keV. We can then use 8% for the left-hand side of Eq. 18 to obtain $F + f \approx 1.1$. By doing this with a single energy source, we are also controlling for any possible changes of the Fano factor. Now, if the Fano factor and the avalanche variance are the only contributing factors, and we assume that $F = 0.2$ for He:CO₂, this implies that $f \approx 0.9$. This means that $f \approx 0.9$ is the minimum value that avalanche variance will obtain, and it will increase as we move to the lower RFTC values in Fig. 12.

While $f \approx 0.9$ is possible, we note that most avalanche distribution models show a lower fractional variance than this at similar reduced field values. Ref. [38] simulates many gas mixtures and they all show the avalanche variance continuing to decrease beyond what we can interpret here. This suggests that there may still be some optimization to be done and optimizing the transfer and collection fields for charge transfer could yield additional improvements. Ref. [39] shows there is indeed an effect on the resolution from the collection field. The ideal study would also have another measurement(s) up to, and beyond, the maximum χ value to see how the resolution responds, possibly repeating this study with a single thin GEM setup. Using additional source energies would allow one to look for deviations in

the expected behavior as a function of energy, which could also point to unaccounted factors affecting the PH resolution.

We note that the resolution for the 2-tGEM setup is slightly greater than for the 3-tGEM setup. This could be related to the difference in the transfer and collection fields, or slight differences between different bottles of gas, or the GEMs themselves. For instance in Ref. [6], a similar double-thin-GEM setup achieves an asymptotic PH resolution of approximately 8.8% with the same proportion of He:CO₂ gas from a different vendor. However, regardless of the exact systematic differences, by minimizing the gain and field-dependent effects, the asymptotic resolution and RFTC can be related in a way that provides a minimum energy resolution value that a GEM-based detector should be able to achieve for a given gas at a given ionization energy.

6. Summary and final remarks

GEMs, as both gas avalanche devices and MPGDs, are becoming more popular in a variety of experimental areas. A comprehensive understanding of the gain they produce and how it affects the energy resolution can be useful when designing GEM-based detectors. This article presented the combined results of extensive gas detector optimization studies for the larger directional nuclear recoil effort currently focusing on dark matter searches. A large data set of different gas mixtures and various GEM-based setups was presented, and a method was sought to explain the data in a more comprehensive way without producing detailed simulations. Following some literature review, we obtain a more complete understanding of the gain and its effect on the energy resolution along the behavior of the involved experimental parameters across the broad parameter space in which GEM-based detectors operate.

A simple and standard way of describing GEM gain data is to say that the gain is strictly exponential with the total voltage applied across the GEMs. This assumption implicitly assumes a somewhat arbitrary threshold model for the gain, i.e. a minimum voltage on the GEMs is required to produce a non-zero gain. While this describes the gain of any single GEM setup well, it can not accommodate changes in gas pressure, GEM thickness, or the number of GEMs. We defined the reduced GEM-averaged quantities to further extend the threshold model to include all of the operational parameters relevant for GEM-based detectors. However, this description still only provides information about these operational detector parameters, and no information about the gas can be inferred.

To proceed, a generalized form for the first Townsend coefficient, combined with the aforementioned reduced GEM-averaged field, is used to show that the threshold model is a special case of a more general description of the gas gain which gives access to information about the particular gas mixture being used. In fact, there are several special cases of this general description and we used multiple data sets, from multiple detector setups, to compare the threshold model with another that is more physically descriptive, providing a measurement of the ionization potential of the gas mixture. Specifically, we found that these two models perform nearly equally well with Ar:CO₂ (70:30) data using two different energy sources, with SF₆ data at

different gas pressures, and with ⁴He:CO₂ (70:30) data recorded with multiple different GEM-based detector setups.

While the design and geometric details of any specific GEM can affect the gain, the first order contribution remains the reduced field and the nearly proportional relationship between the reduced first Townsend coefficient and the GEM-average reduced field is robust. While the entire individual ⁴He:CO₂ (70:30) data sets are not well described, we showed that the asymptotic (high) gain performance of each can be predicted quite well.

Detector operation near the asymptotic gain, above any noise from the readout electronics, is an important regime to study for experiments concerned with low-energy, rare event, searches. We note the self-consistency of the results shown here, and the attention given to the many systematic effects. With more study, particularly focused on keeping the systematic uncertainties low, the slight deviations from the strictly exponential behavior of the gain on the total voltage across the GEMs could be further constrained.

We also exploited the fact that a non-segmented readout, i.e. the conductive charge collection plate, reduces the PH resolution to three terms. First, a noise term related to the analog readout electronics which can be suppressed by operating the detector at its asymptotic gain, and the other two terms involve the Fano factor and the variance of the charge avalanche distribution. By using only the asymptotic gain values from multiple detector setups with a single gas mixture, ⁴He:CO₂ (70:30), and a single energy source, ⁵⁵Fe to control for the Fano factor, we provided a simple method to estimate at which reduced field value the PH resolution should reach a minimum. After minimizing the detector noise term, we attribute the further decrease in the PH resolution to the decreasing variance in the avalanche distribution as the reduced field increases.

This method essentially allows one to determine if, and by how much, the PH resolution can be improved by changing the gain. It is not necessarily intuitive but, in terms of the PH resolution, using fewer GEMs to achieve a desired SNR is generally better than using more, and individual GEMs produced with materials capable of maintaining higher electric fields would be preferred. This is because, for equal gains, a setup with more GEMs operates at a lower GEM-averaged reduced field. And, at lower reduced fields, one can generally expect the variance of the charge avalanche distribution to be larger. This will in turn increase the PH resolution, assuming all other effects have been accounted for. While it is not straightforward, this effect seems to be inconsequential in the reduced field ranges that thinner GEMs, e.g 50 μm, typically operate, while more drastic in the operating range of THGEMs, e.g 400 μm, where the avalanche variance is larger. After correcting for time variations, a simple method for determining the minimum energy resolution achievable in GEM-based detectors for a given gas at a given initial ionization energy was also described.

We also presented our group's first positive results with SF₆, a Negative Ion (NI) gas. These are particularly interesting within the directional dark matter community which seeks to lower diffusion in the drift region, thus enhancing the ability to record individual nuclear recoil ionization tracks and extract a

definitive directional dark matter signature. However regardless of the exact application, the results shown here provide a good overview of the gain, its effect on the energy resolution, and the contributing experimental parameters when considering any GEM-based detector.

Acknowledgements

We would like to thank the machine shop at the University of Hawaii, Department of Physics & Astronomy for their help with manufacturing of the many detector components. We would also like to thank Majd Ghreer for his useful feedback on the manuscript. We acknowledge support from the U.S. Department of Homeland Security under Award Number 2011-DN-077-ARI050-03 and the U.S. Department of Energy under Award Numbers DE-SC0007852, DE-SC0010504, and DE-SC0018034.

7. References

References

- [1] F. Sauli, *GEM: A new concept for electron amplification in gas detectors*, *Nucl. Instrum. Meth. A* **386** (1997) 531.
- [2] J. N. Marx and D. R. Nygren, *The Time Projection Chamber*, *Phys. Today* **31N10** (1978) 46.
- [3] ALICE collaboration, *ALICE TPC upgrade for High-Rate operations*, *PoS ICFAQGP2015* (2017) 094 [1511.04988].
- [4] B. Ketzer, Q. Weitzel, S. Paul, F. Sauli and L. Ropelewski, *Performance of triple GEM tracking detectors in the COMPASS experiment*, *Nucl. Instrum. Meth. A* **535** (2004) 314.
- [5] J. A. Merlin, *Study of long-term sustained operation of gaseous detectors for the high rate environment in CMS*, Ph.D. thesis, Strasbourg U., 4, 2016.
- [6] S. Vahsen, M. Hedges, I. Jaegle, S. Ross, I. Seong, T. Thorpe et al., *3-D tracking in a miniature time projection chamber*, *Nucl. Instrum. Meth. A* **788** (2015) 95 [1407.7013].
- [7] I. Jaegle et al., *Compact, directional neutron detectors capable of high-resolution nuclear recoil imaging*, *Nucl. Instrum. Meth. A* **945** (2019) 162296 [1901.06657].
- [8] P. Lewis et al., *First Measurements of Beam Backgrounds at SuperKEKB*, *Nucl. Instrum. Meth. A* **914** (2019) 69 [1802.01366].
- [9] S. Vahsen, H. Feng, M. Garcia-Sciveres, I. Jaegle, J. Kadyk et al., *The Directional Dark Matter Detector (D^3)*, *EASPUB* **53** (2012) 43 [1110.3401].
- [10] T. Kim, M. Freytsis, J. Button-Shafer, J. Kadyk, S. E. Vahsen and W. A. Wenzel, *Readout of TPC tracking chambers with GEMs and pixel chip*, *Nucl. Instrum. Meth. A* **589** (2008) 173.
- [11] S. Vahsen, K. Oliver-Mallory, M. Lopez-Thibodeaux, J. Kadyk and M. Garcia-Sciveres, *Tests of gases in a mini-TPC with pixel chip readout*, *Nucl. Instrum. Meth. A* **738** (2014) 111.
- [12] P. Lewis, S. Vahsen, I. Seong, M. Hedges, I. Jaegle and T. Thorpe, *Absolute Position Measurement in a Gas Time Projection Chamber via Transverse Diffusion of Drift Charge*, *Nucl. Instrum. Meth. A* **789** (2015) 81 [1410.1131].
- [13] S. E. Vahsen et al., *CYGNUS: Feasibility of a nuclear recoil observatory with directional sensitivity to dark matter and neutrinos*, 2008.12587.
- [14] S. E. Vahsen, C. A. J. O'Hare and D. Loomba, *Directional recoil detection*, *Ann. Rev. Nucl. Part. Sci.* **71** (2021) 189 [2102.04596].
- [15] T. N. Thorpe, *Gain resolution studies and first dark matter search with novel 3D nuclear recoil detectors*, Ph.D. thesis, Hawaii U., 2018.
- [16] R. Veenhof, "Garfield++ webpage at CERN." <https://garfieldpp.web.cern.ch/garfieldpp/>.
- [17] B. Morgan, A. M. Green and N. J. Spooner, *Directional statistics for WIMP direct detection*, *Phys. Rev. D* **71** (2005) 103507 [astro-ph/0408047].
- [18] D. N. Spergel, *The Motion of the Earth and the Detection of Wimps*, *Phys. Rev. D* **37** (1988) 1353.
- [19] C. Martoff, D. Snowden-Ifft, T. Ohnuki, N. Spooner and M. Lehner, *Suppressing drift chamber diffusion without magnetic field*, *Nucl. Instrum. Meth. A* **440** (2000) 355.
- [20] D. Snowden-Ifft, C. Martoff and J. Burwell, *Low pressure negative ion drift chamber for dark matter search*, *Phys. Rev. D* **61** (2000) 101301 [astro-ph/9904064].
- [21] DRIFT collaboration, *First background-free limit from a directional dark matter experiment: results from a fully fiducialised DRIFT detector*, *Phys. Dark Univ.* **9-10** (2015) 1 [1410.7821].
- [22] N. Phan, R. Lafler, R. Lauer, E. Lee, D. Loomba, J. Matthews et al., *The novel properties of SF₆ for directional dark matter experiments*, *JINST* **12** (2017) P02012 [1609.05249].
- [23] P. Lewis, M. Hedges, I. Jaegle, I. Seong, J. Schueler, T. Thorpe et al., *Primary track recovery in high-resolution gas time projection chambers, (in preparation for EPJC)* (2021).
- [24] P. Sorensen, M. Heffner, A. Bernstein, J. Renner and M. Sweany, *Towards energy resolution at the statistical limit from a negative ion time projection chamber*, *Nucl. Instrum. Meth. A* **686** (2012) 106 [1205.6427].
- [25] T. Aoyama, *Generalized gas gain formula for proportional counters*, *Nuclear Instruments and Methods in Physics Research Section A: Accelerators, Spectrometers, Detectors and Associated Equipment* **234** (1985) 125.
- [26] W. Diethorn, *A methane proportional counter system for natural radiocarbon measurements (thesis)*, .
- [27] A. Williams and R. Sara, *Parameters affecting the resolution of a proportional counter*, *The International Journal of Applied Radiation and Isotopes* **13** (1962) 229.
- [28] A. Zastawny, *Gas amplification in a proportional counter with carbon dioxide*, *Journal of Scientific Instruments* **43** (1966) 179.
- [29] H. Schlumbohm, *Zur Statistik der Elektronenlawinen im ebenen Feld. III*, *Zeitschrift fur Physik* **151** (1958) 563.
- [30] G. Alkhozov, *Statistics of electron avalanches and ultimate resolution of proportional counters*, *Nucl. Instrum. Meth.* **89** (1970) 155.
- [31] G. Knoll, *Radiation Detection and Measurement (4th ed.)*. John Wiley, Hoboken, NJ, 2010.
- [32] K. Bronić, *W values and Fano factors for electrons in rare gases and rare gas mixtures.*, *Ionizing Radiation (Hoshasen)* (1998).
- [33] A. Engel, *Ionized Gases*. AIP-Press, 01, 1994.
- [34] A. Sharma, *Properties of some gas mixtures used in tracking detectors*, .
- [35] I. Lopes, H. Hilmert and W. F. Schmidt, *Ionisation of gaseous and liquid sulphur hexafluoride by ⁶⁰Co γ -radiation*, *Journal of Physics D: Applied Physics* .
- [36] H. Ishiura, R. Veenhof, K. Miuchi and I. Tomonori, *MPGD simulation in negative-ion gas for direction-sensitive dark matter searches*, *J. Phys. Conf. Ser.* **1498** (2020) 012018 [1907.12729].
- [37] H. Raether, *Electron avalanches and breakdown in gases*. Butterworths, 01, 1964.
- [38] H. Schindler, S. F. Biagi and R. Veenhof, *Calculation of gas gain fluctuations in uniform fields*, *Nucl. Instrum. Meth. A* **624** (2010) 78.
- [39] G. P. Guedes, A. Breskin, R. Chechik and D. Mormann, *Effects of the induction-gap parameters on the signal in a double-GEM detector*, *Nucl. Instrum. Meth. A* **497** (2003) 305.